CHAPTER 4

VERIFICATION OF THE CHF MODEL

4.1 Comparison with the Experimental Data

To verify the accuracy of the proposed model, a big CHF database has been gathered. The detailed information is shown in the Appendix 1. The database comes from three sources. The first is Celata database (1994b), which was used by Celata to verify his model (1994a), including 1887 data points. The database covers the following working range that is characterized by the high mass flux condition.

$$0.9 \le G \le 90Mg/m^2s;\ 0.09 \le P \le 8.4MPa;\ 19 \le \Delta T_{in} \le 237K;\ 0.3 \le D \le 25.4mm.$$

The second is Pei database (1983), which was used by Weisman-Pei to test their bubble-crowding model, including 486 data points and covering the following range that is characterized by the high-pressure condition.

$$0.9 \le G \le 18.6Mg/m^2s;\ 2.17 \le P \le 19.25MPa;\ 5.3 \le \Delta T_{in} \le 354;\ 1.1 \le D \le 37.5mm.$$

The third is a new database presented by Chen et al (1997). The database includes 109 data points and is characterized by low to medium pressure and low mass flux condition.

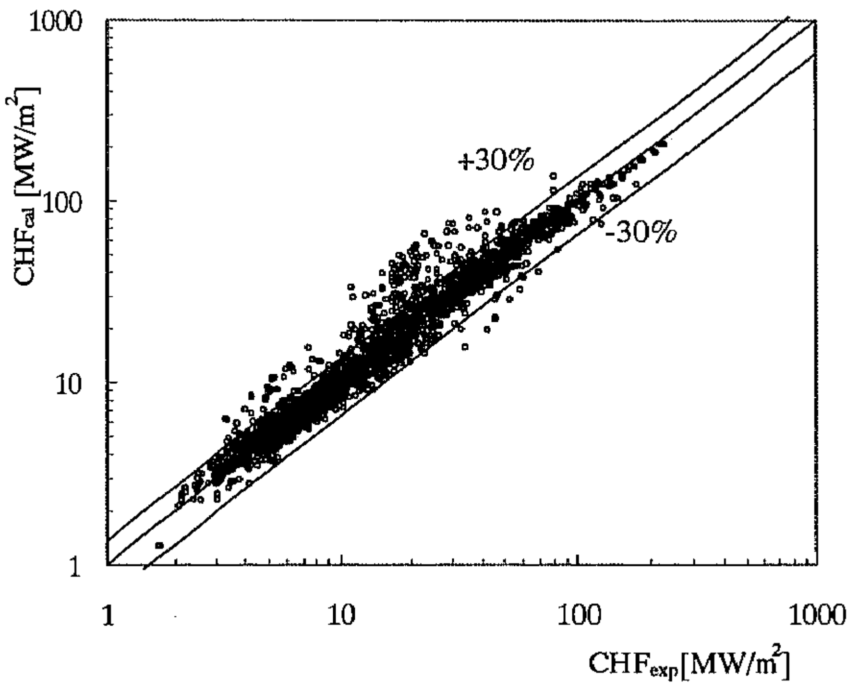

Fig.4-1 Calculated versus Experimental CHF

Therefore, the whole data used for the model verification include 2482 data points and covers the following working scopes. The whole database covers almost the entire physics scope.

$0.9 \le G \le 90Mg/m^2s$; $0.09 \le P \le 19.25MPa$;

$5.3 \le \Delta T_{in} \le 354K$; $0.3 \le D \le 37.5mm$

Figure 4-1 shows a comparison of calculated versus experimental CHF, using the above databases. About 89.6% of the data are predicted within $\pm 30\%$. The verification shows the proposed model is valid through a wide range of operating condition.

With reference to the model raised by Celata (1994a), comparisons for the CHF general prediction ability between the Celata model and the present model are accomplished. The percentage of data points calculated with a given error band (%) is plotted, against the error band, using the Celata database only, Pei database only and all the databases. Although the present model prediction does not show a better prediction ability than the Celata model with using only the Celata database in fig.4-2, it shows a much better prediction with using only the Pei database (fig.4-3) and a general better prediction than the Celata model is obtained with using all the databases (fig.4-4).

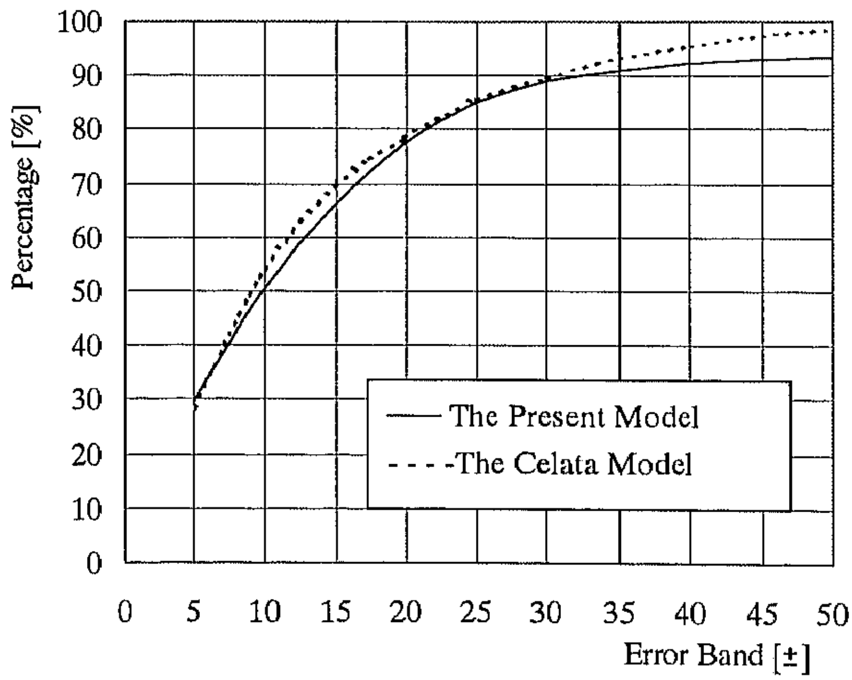

Fig.4-2 Comparisons of the CHF Prediction Ability between the Present Model and the Celata Model with Using only the Celata Database

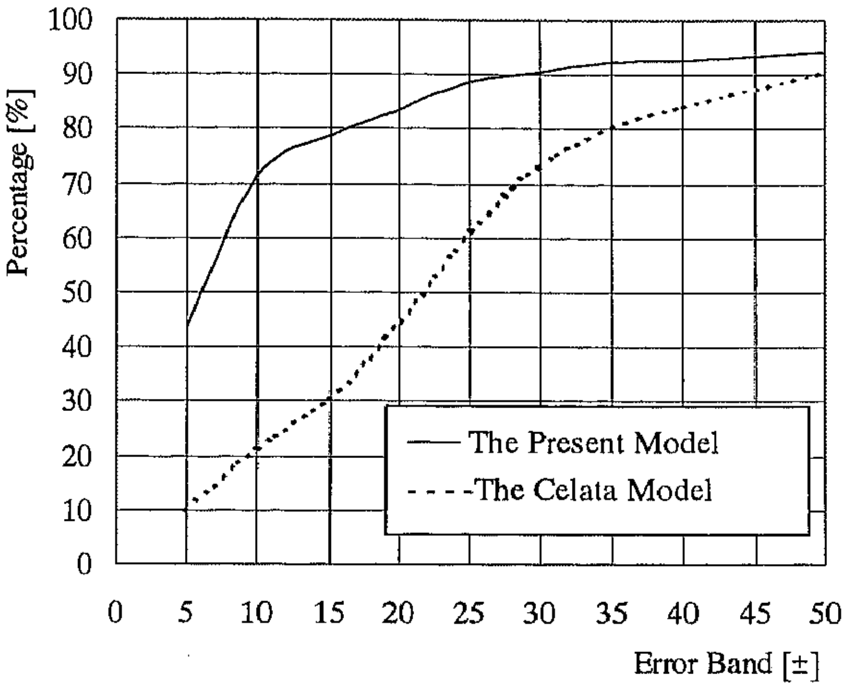

Fig.4-3 Comparisons of the CHF Prediction Ability between the Present Model and the Celata Model with Using only the Weisman-Pei Database

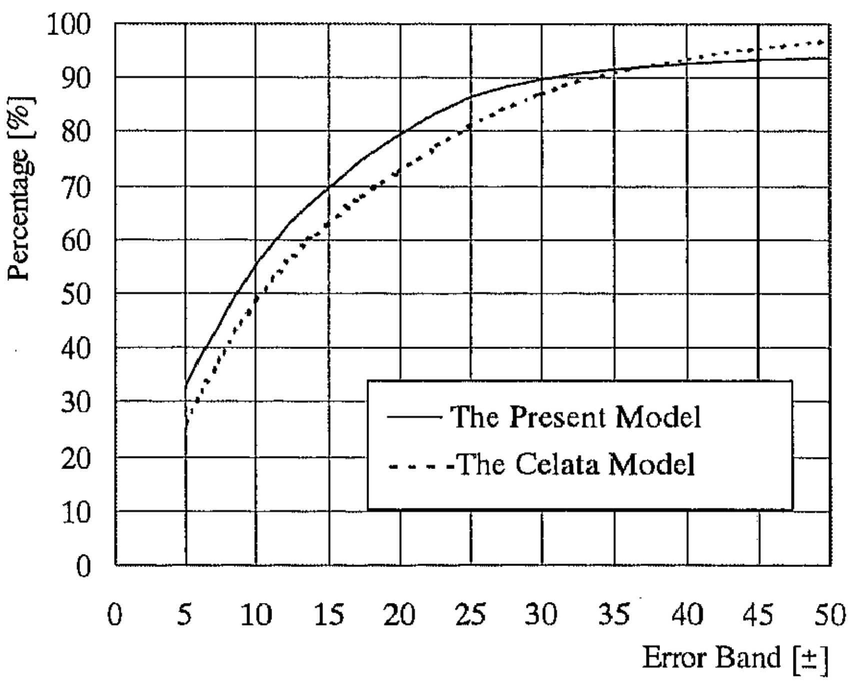

Fig.4-4 Comparisons of the CHF Prediction Ability between the Present Model and the Celata Model with Using all the Databases

It has to be specified that, with different model adoptions for the NVG point, true quality and void fraction, the proposed model gives different prediction result. All the listed results are got with the model adoptions same as that shown in the Appendix 3. The model selection is based on the analysis carried out in chapter 6.1. With the changing of the models for the NVG point, true quality and void fraction, the proposed model may give even better prediction (for example, with replacing the Ahmad model for the true quality by the Jafri model; or at low L/D condition, replacing the Ahmad void fraction model by the Dix model).

Another thing must be mentioned is that under some extreme conditions, such as at high pressure ($P \geq 17.5$ MPa, Bortoli data, 1958) or high mass flux ($G \geq 50000$ kg/m^{2}s, with CHF up to 100 MW/m^2, Ornatsukii data, 1960, 1965), with the proposed model, sometimes the final calculated q doesn't equal to the assumed q_m even when the assumed q_m has converged to a point. This converging q_m value is always the lowest possible CHF value, which is the heat flux needed for the NVG point establishment at the tube exit. The unpredictability and the converging process may imply that the CHF under such circumstance happens before the NVG point is established due to the change of the CHF triggering mechanism.

Actually, the CHF under such circumstance can be calculated by doing a little modification to the Levy D_B (by increasing D_B step by step,). That is to say, if we cannot calculate CHF with the original Levy D_B, we increase D_B as $D_B=1.01D_B$ and repeat the calculation procedure. If CHF still cannot be got, increase D_B as $DB=1.02D_B$.... until the CHF is reached. Generally, the CHF can be got within $D_B<1.5D_{B\text{-}Levy}$. The calculated CHF is actually the heat flux needed for the establishment of the NVG point at the tube exit (q_{NVG}), that is, the lowest possible heat flux needed for the establishment of the first kind of subcooled flow boiling. The method is tested with Bortoli 's data (1958, for high pressure condition) and Ornatsukii 's data (1965, 1960, for high G condition). The result is astonished good, which may imply that, under such high G or high P condition, the CHF occurs before and near the NVG point due to the change of the CHF triggering mechanism, which is a consequent result of the change of the flow pattern (The first kind of flow pattern is replaced by the second kind of flow pattern). Corresponding detailed analysis is discussed in chapter 6.3.

4.2 Comparisons of the Present Model with the Celata Model

So far, the Celata model can be said to be the best model for the CHF prediction. In the following, comparisons for the prediction of the CHF and important parameters are accomplished over a wide scope. In the figures, solid and broken lines represent the prediction results from the present model and the Celata model respectively.

4.2.1 Comparisons of the CHF Prediction

Figures 4-5 ~ 4-10 show the comparisons of the predicted CHF from the present and the Celata models with compared to the experimental data under 6 different working conditions. From the figures, we can see that at low pressure, the two models give almost the same CHF predictions although the basic thought of the two models divers greatly. At high pressure, the Celata model has a tendency of giving a little worse prediction.

4.2.2 Comparisons of U_B (Figs. 4-11 ~ 4-16) and δ (Figs. 4-17 ~ 4-22)

The calculation of U_B and δ is the main difference between the two models. The present model considers gas and liquid phases separately. With the assumption that the same wavelength at the two liquid-gas interfaces, the U_B is calculated firstly. The δ is calculated on the base of the U_B. Celata gave the δ as superheated layer thickness minus vapor blanket diameter. In the Celata model, U_B is obtained on the base of the δ. It is interesting to see that U_B and δ are obtained with no big difference existing even though the calculation process differs greatly.

4.2.3 Comparisons of D_B and L_B (Figs.4-17 ~ 4-22)

In the D_B calculation, Celata adopted the Staub (1969) model, in which D_B is inversely proportional to G^2. The present model adopted the Levy model, in which D_B is inversely proportional to G. As to the L_B calculation, two models both employed the Helmholtz instability wavelength that is inversely proportional to U_B^2.

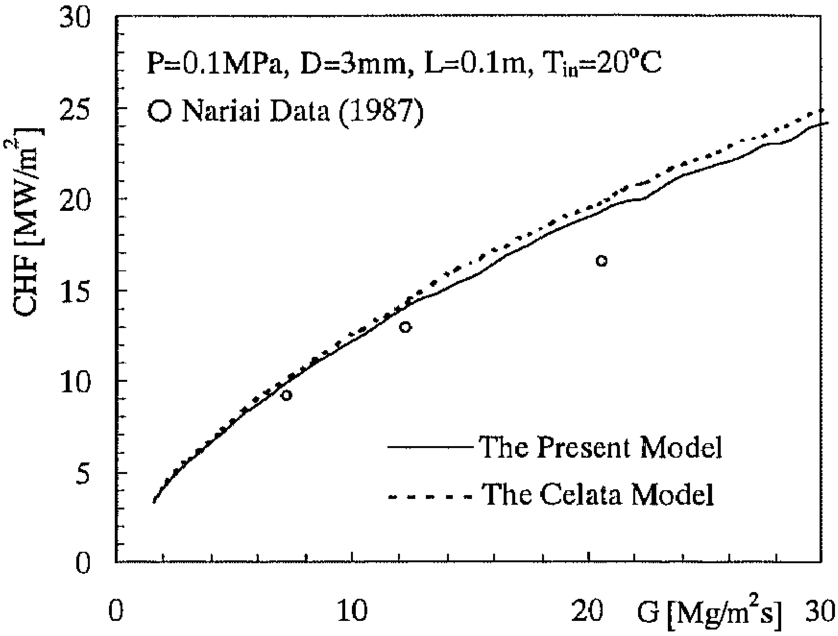

Fig.4-5 Comparisons of the CHF between the Present Model and the Celata Model at P=0.1MPa

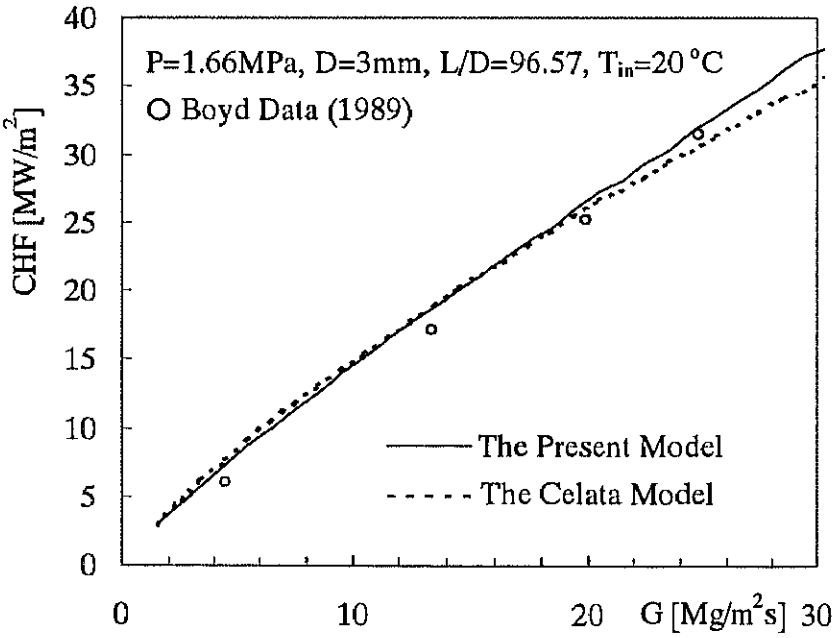

Fig.4-6 Comparisons of the CHF between the Present Model and the Celata Model at P=1.66 MPa

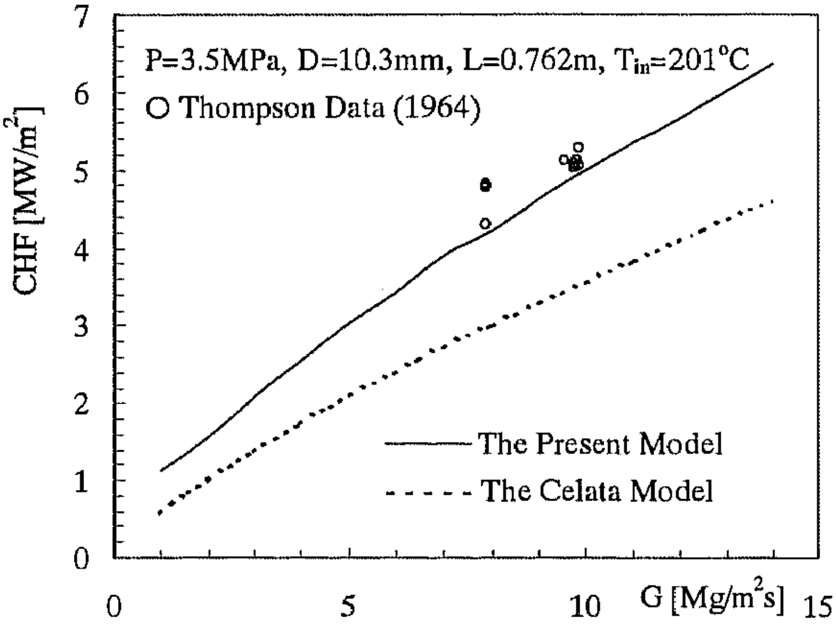

Fig.4-7 Comparisons of the CHF between the Present Model and the Celata Model at P=3.5 MPa

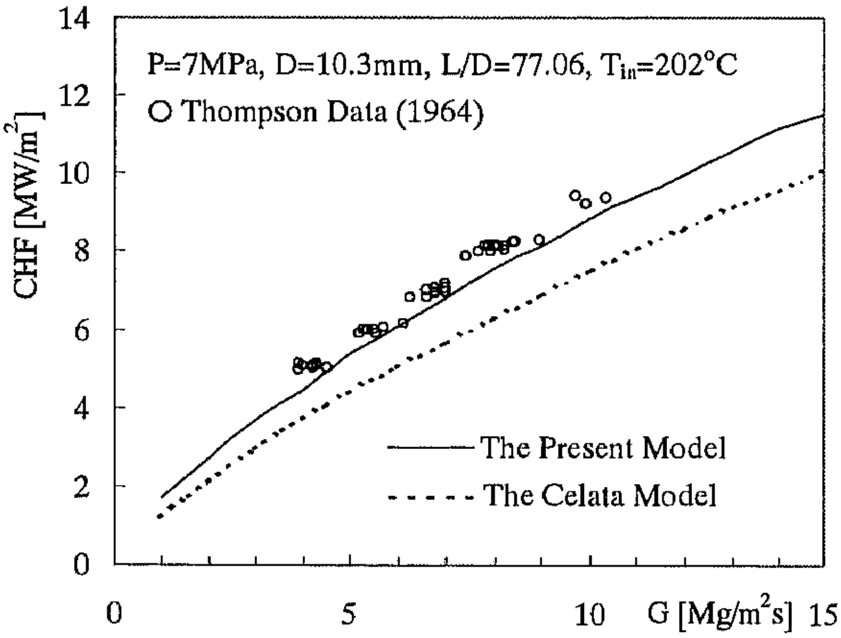

Fig.4-8 Comparisons of the CHF between the Present Model and the Celata Model at P=7 MPa

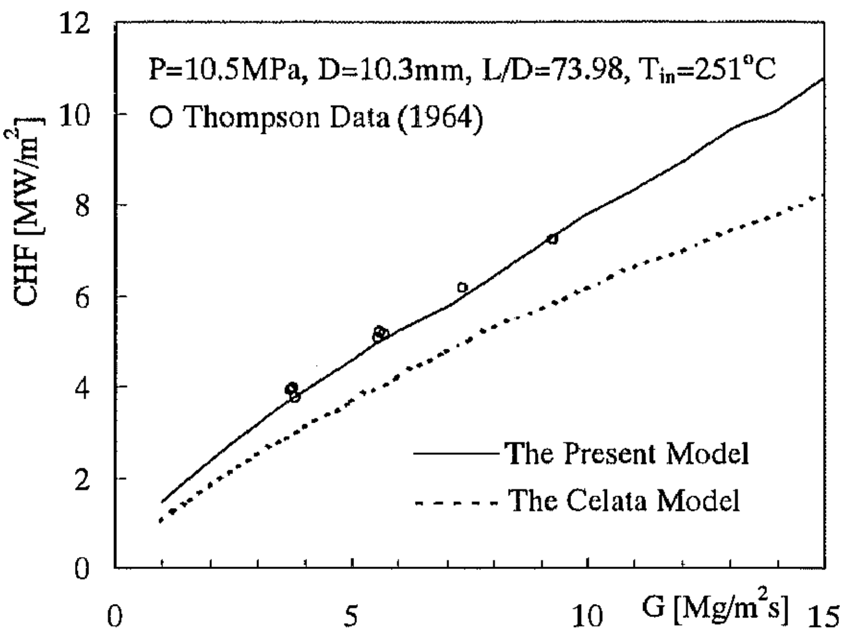

Fig.4-9 Comparisons of the CHF between the Present Model and the Celata Model at P=10.5 MPa

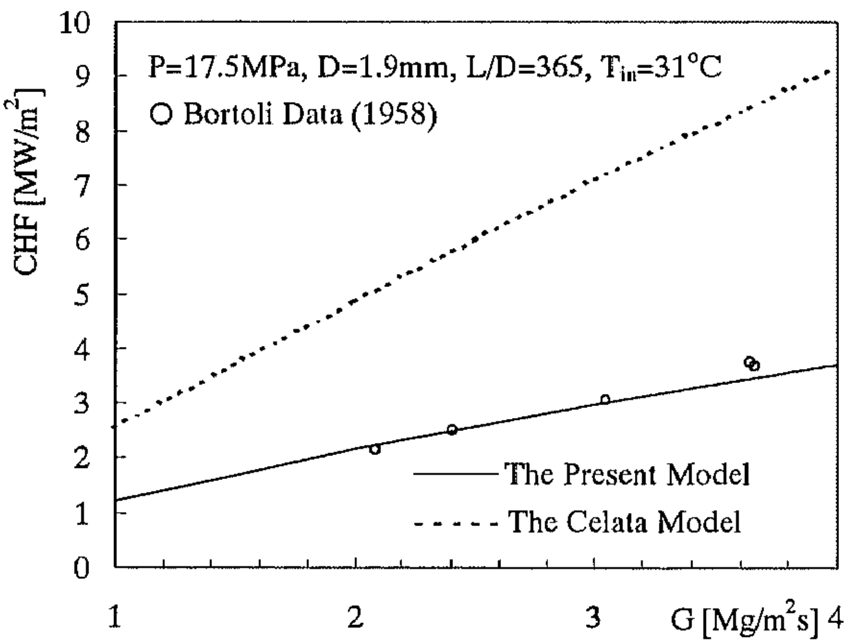

Fig.4-10 Comparisons of the CHF Prediction between the Present Model and the Celata Model at P=17.5 MPa

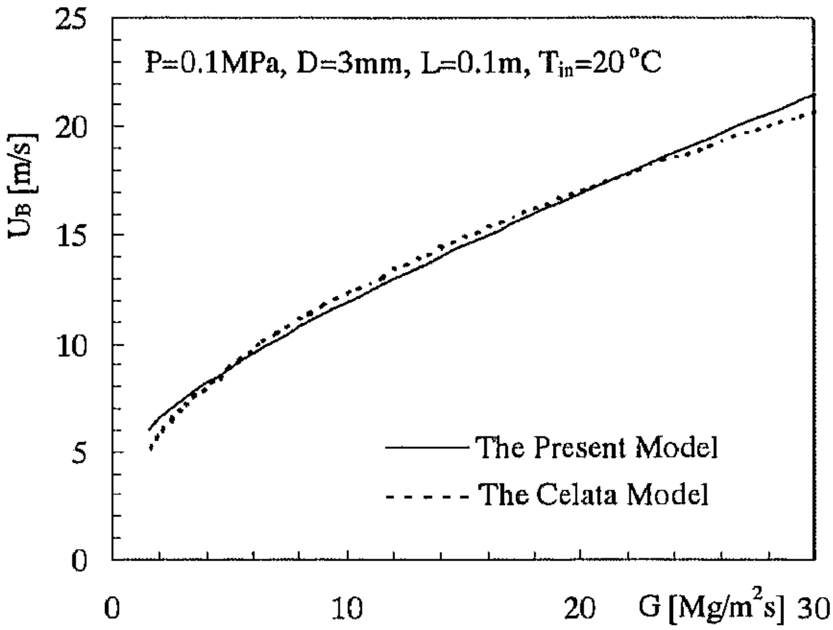

Fig.4-11 Comparisons of the Vapor Blanket Velocity U_B between the Present Model and the Celata Model at P=0.1MPa

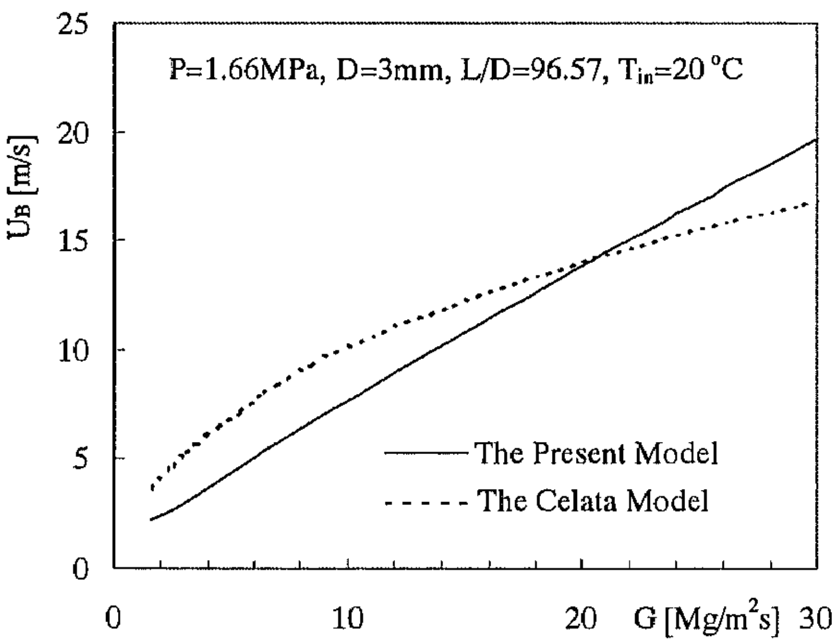

Fig.4-12 Comparisons of the Vapor Blanket Velocity U_B between the Present Model and the Celata Model at P=1.66MPa

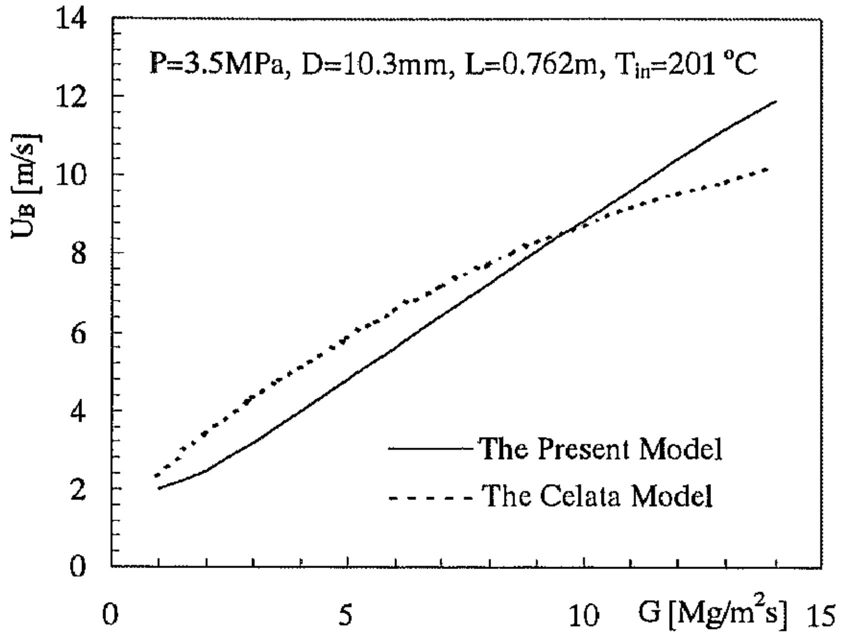

Fig.4-13 Comparisons of the Vapor Blanket Velocity U_B between the Present Model and the Celata Model at P=3.5MPa

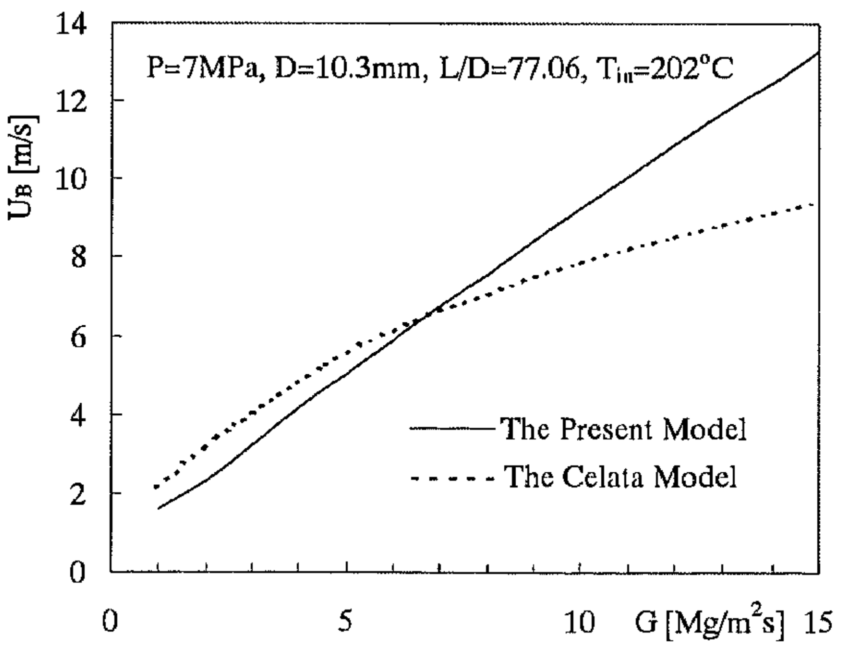

Fig.4-14 Comparisons of the Vapor Blanket Velocity U_B between the Present Model and the Celata Model at P=7MPa

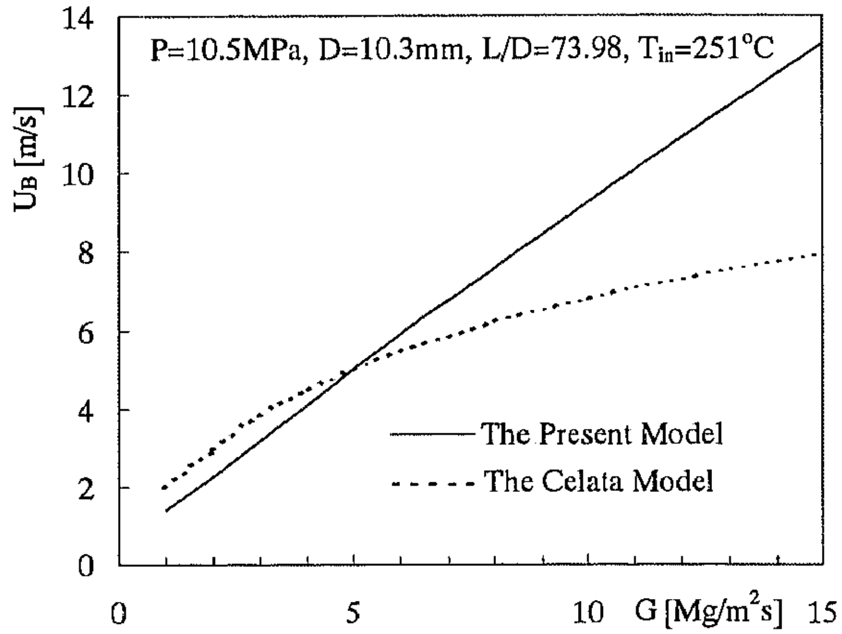

Fig.4-15 Comparisons of the Vapor Blanket Velocity U_B between the Present Model and the Celata Model at P=10.5MPa

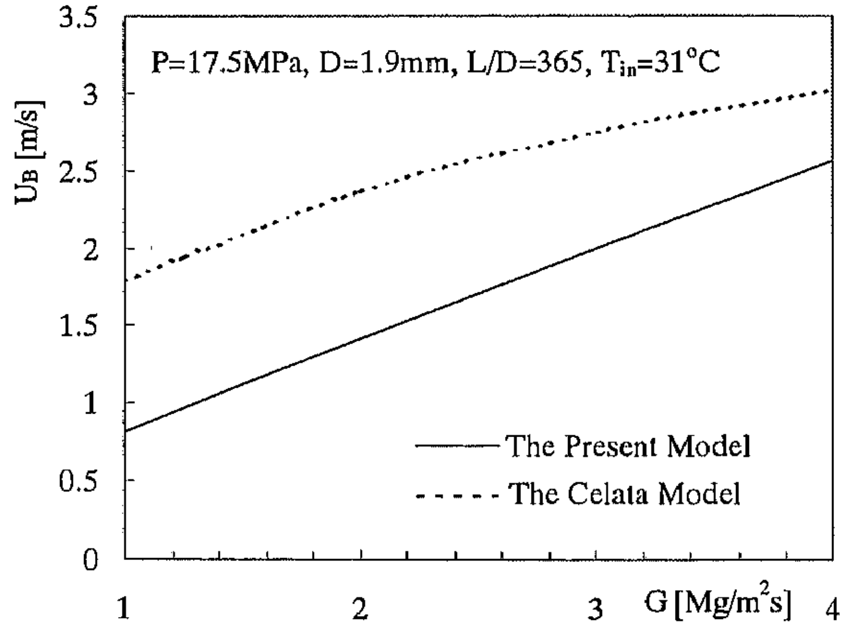

Fig.4-16 Comparisons of the Vapor Blanket Velocity U_B between the Present Model and the Celata Model at P=17.5MPa

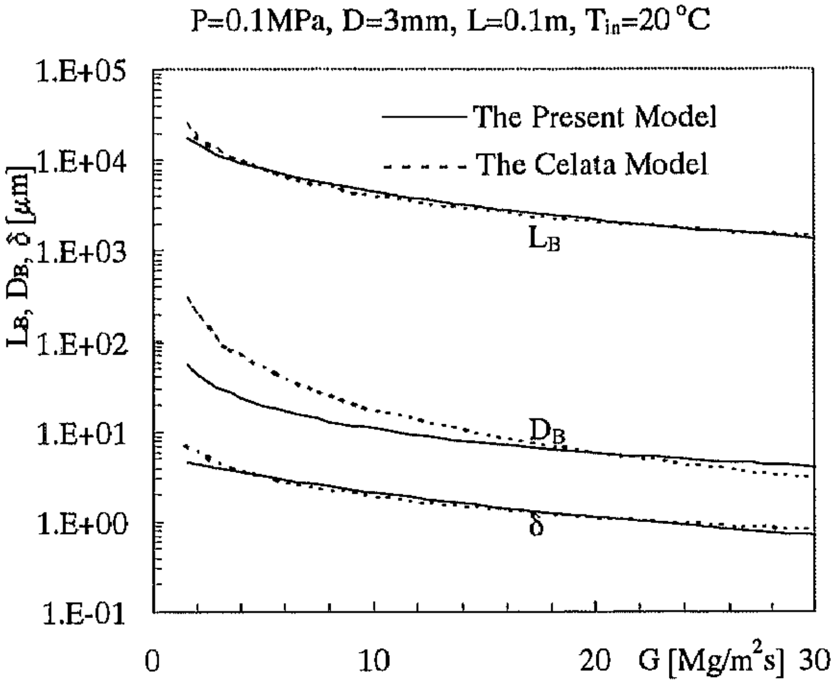

Fig.4-17 Comparisons of the L_B, D_B and δ between the Present Model and the Celata Model at P=0.1MPa

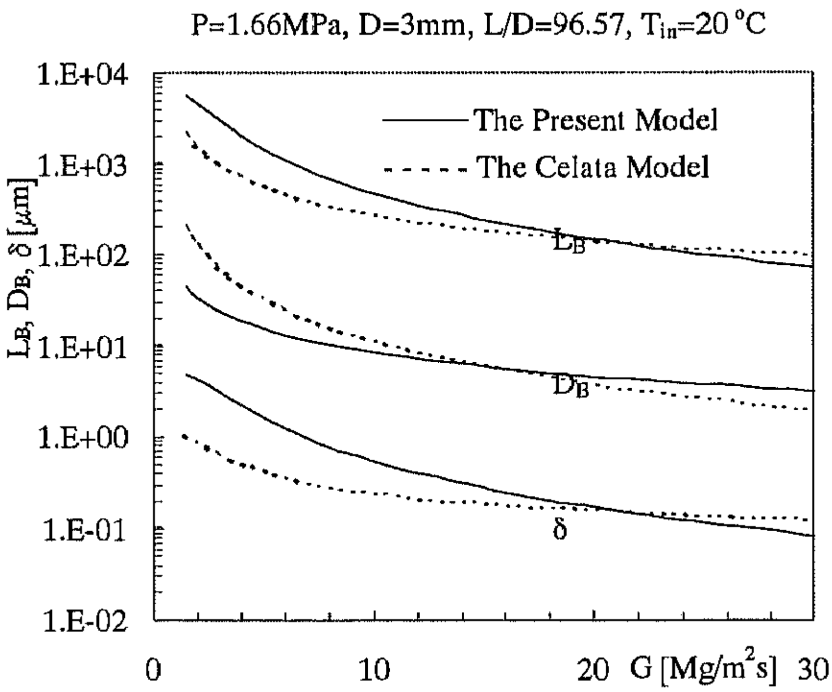

Fig.4-18 Comparisons of the L_B, D_B and δ between the Present Model and the Celata Model at P=1.66MPa

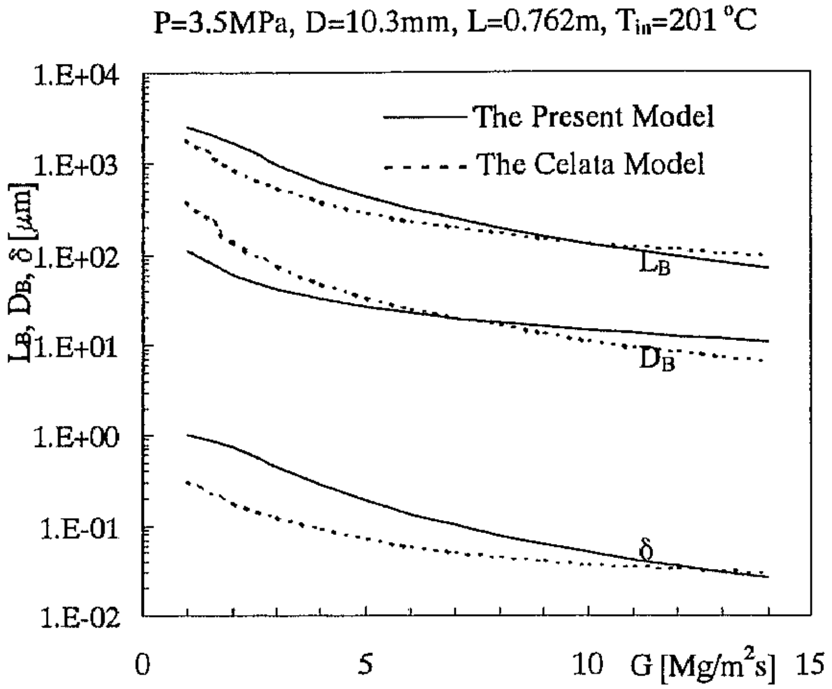

Fig.4-19 Comparisons of the L_B, D_B, δ between the Present Model and the Celata Model at P=3.5MPa

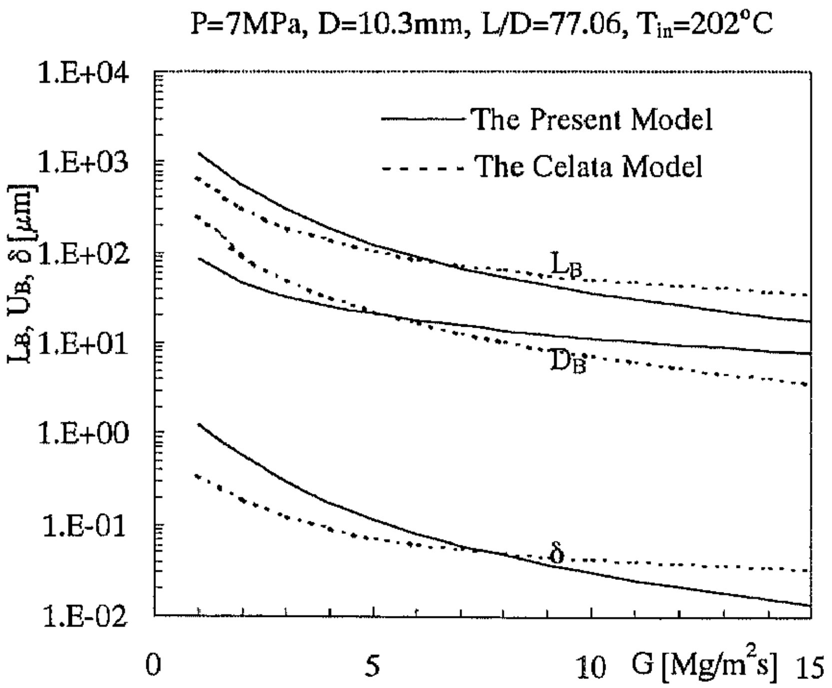

Fig.4-20 Comparisons of the L_B, D_B, δ between the Present Model and the Celata Model at P=7MPa

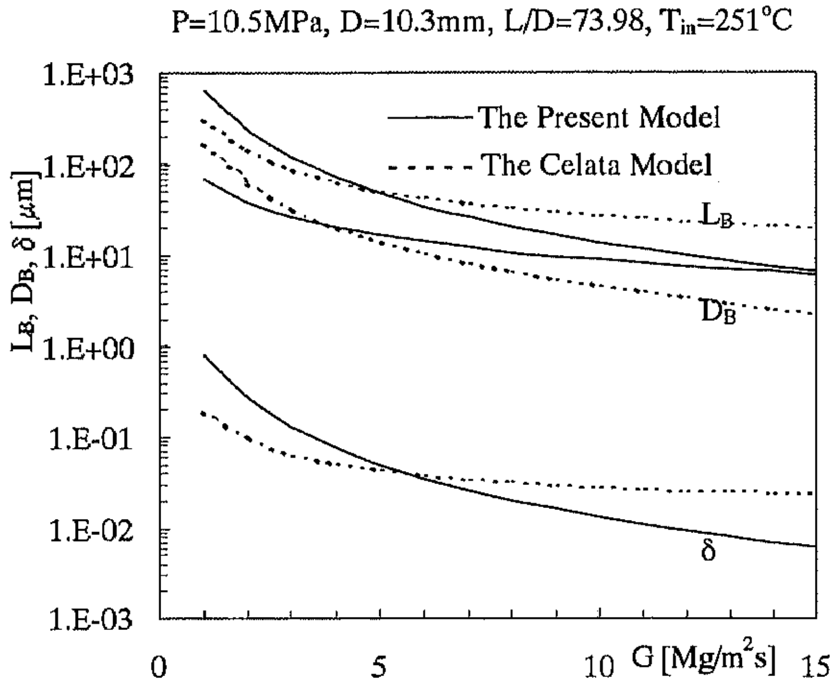

Fig.4-21 Comparisons of the L_B, D_B, δ between the Present Model and the Celata Model at P=10.5MPa

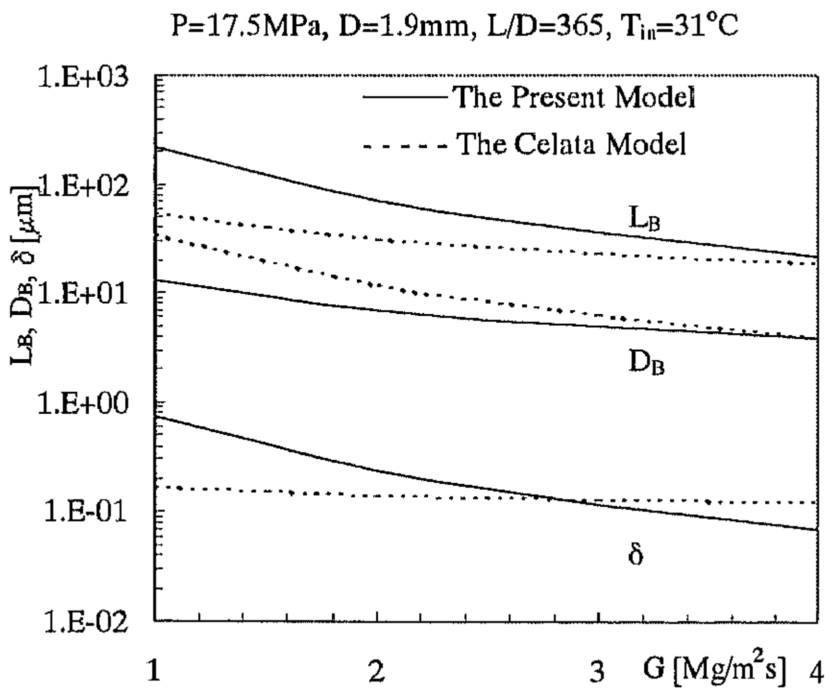

Fig.4-22 Comparisons of the L_B, D_B, δ between the Present Model and the Celata Model at P=17.5MPa

4.3 Systematic Effects of Thermal Hydraulic Conditions and Geometric Parameters in the Model Behavior

4.3.1 Systematic Effects Analysis

Figures 4-23 through 4-28 show the ratio of the calculated CHF to the experimental CHF versus the mass flux, pressure, inlet subcooling, exit equilibrium quality, inner diameter and ratio of heated length to diameter, to ascertain possible systematic effects in the model behavior. No systematic errors of CHF prediction versus the mass flux G (fig.4-23), pressure P (fig.4-24), inlet subcooling ΔT_{in} (fig.4-25), exit equilibrium quality χ_{eqout} (fig.4-26) and inner diameter D (fig.4-27) are observed. But an over-prediction tendency is observed at low L/D (L/D<20, fig.4-28), especially at the high system pressure condition. An analysis is carried out for the prediction of the low L/D data.

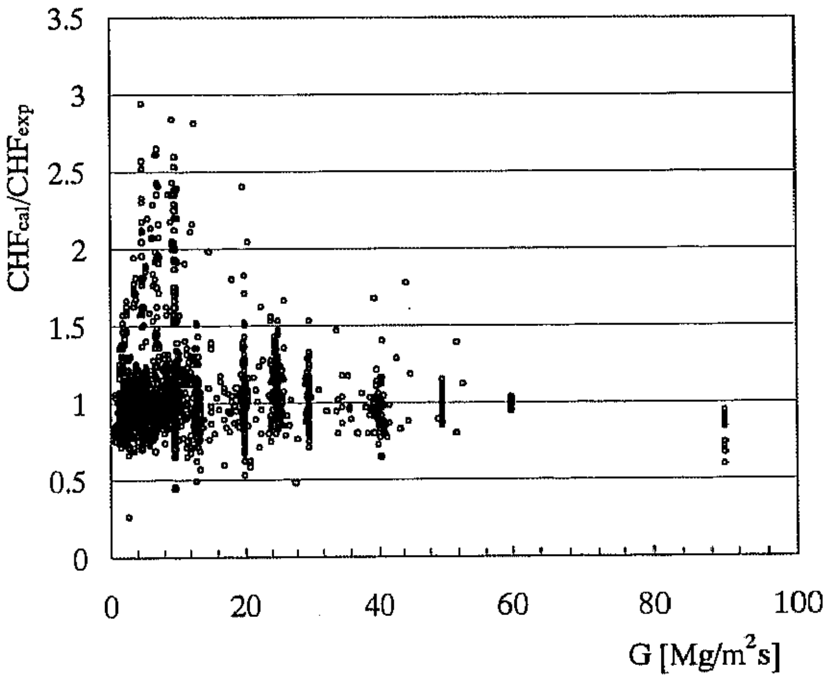

Fig.4-23 Ratio of the Calculated to Experimental CHF versus Mass Flux

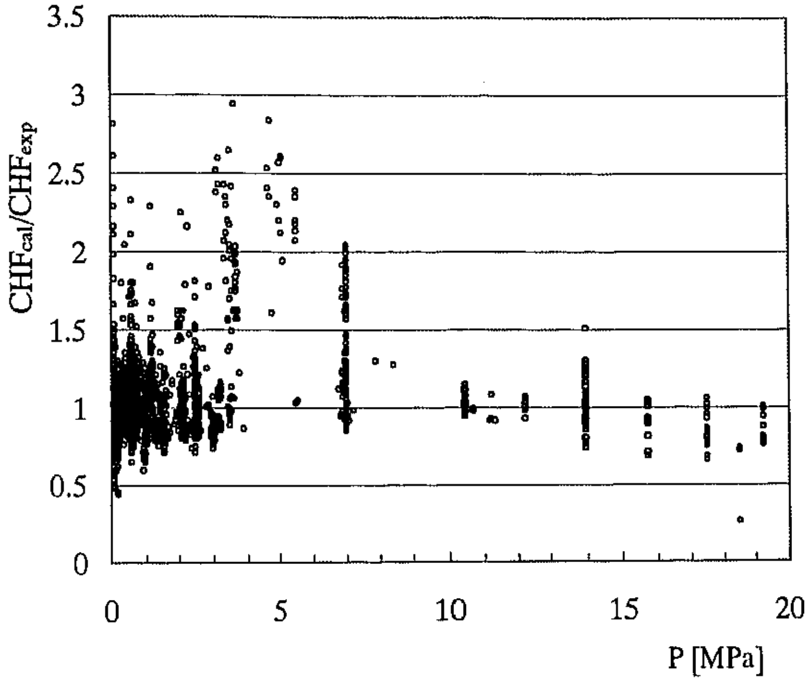

Fig.4-24 Ratio of the Calculated to Experimental CHF versus Pressure

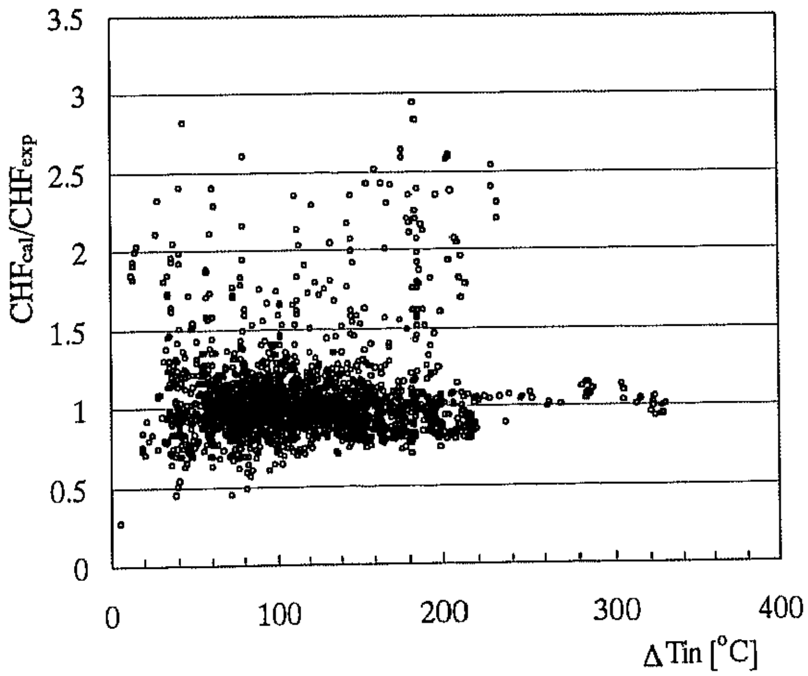

Fig.4-25 Ratio of the Calculated to Experimental CHF versus Inlet Subcooling

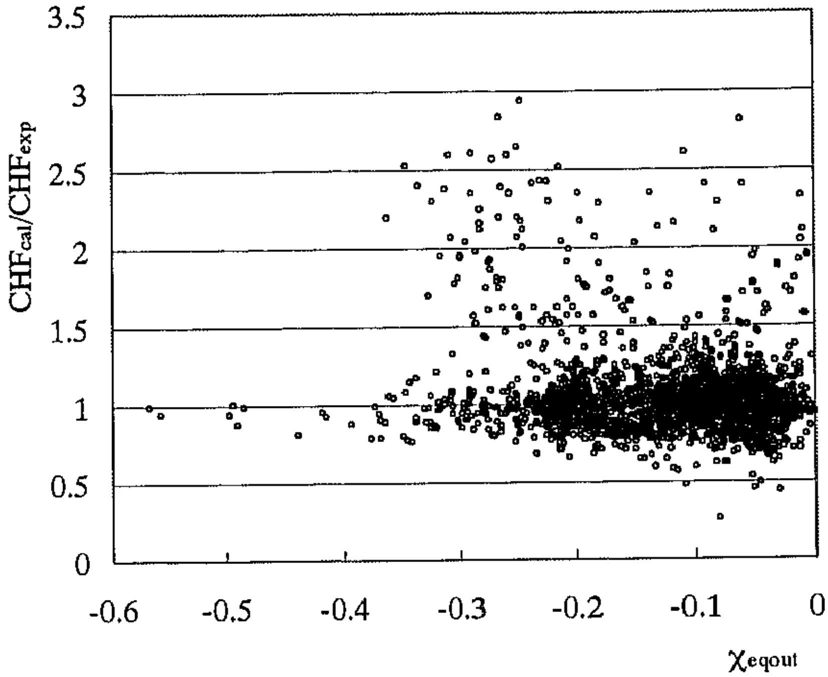

Fig.4-26 Ratio of the Calculated to Experimental CHF versus Exit Equilibrium Quality

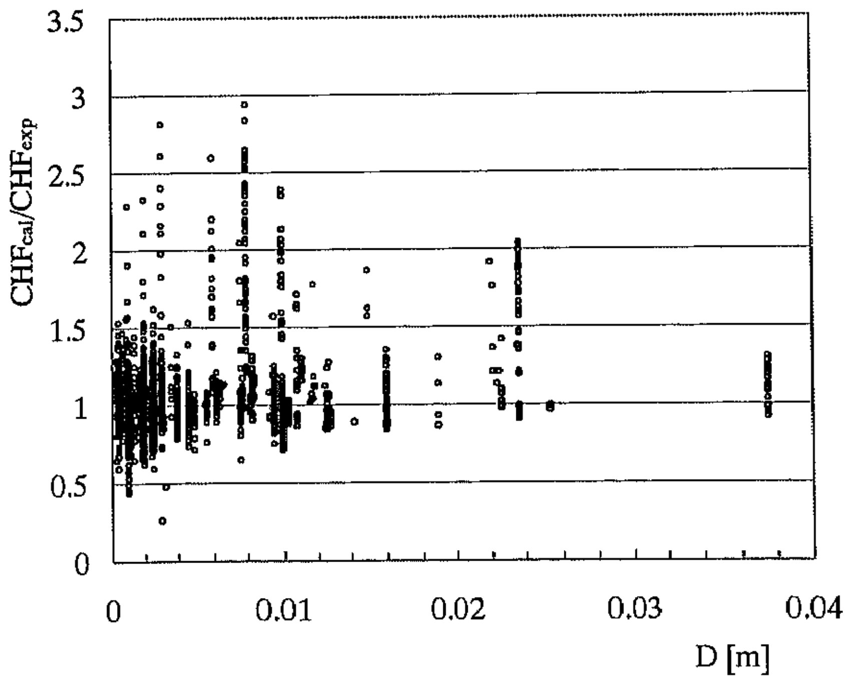

Fig.4-27 Ratio of the Calculated to Experimental CHF versus Inner Diameter

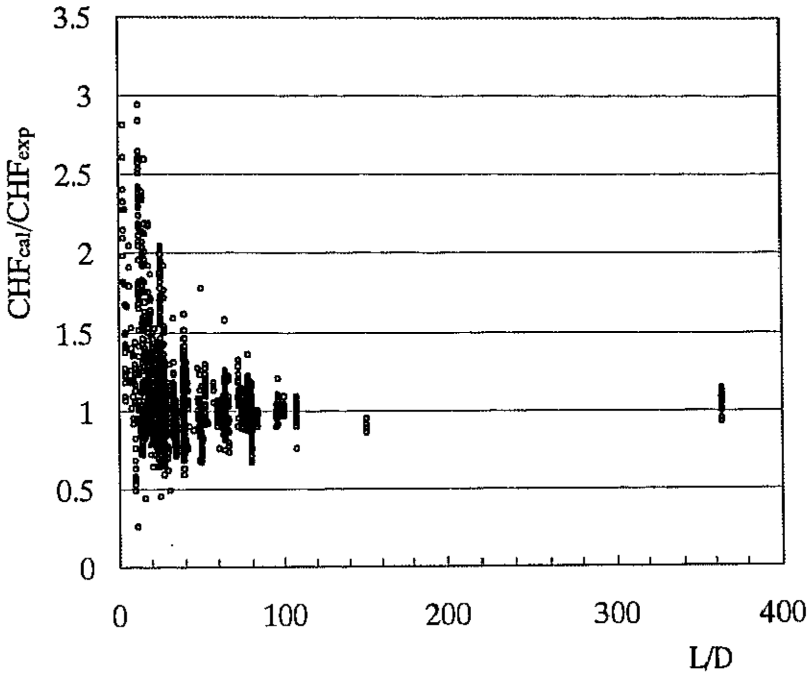

Fig.4-28 Ratio of the Calculated to Experimental CHF versus Ratio of the Heated Length to Tube Diameter

4.3.2 Analysis to Low L/D Data

As mentioned above, the present model shows an over-prediction tendency at low L/D condition. An analysis to the low L/D data is carried out with the result shown in fig.4-29. From the figure, we can get that:

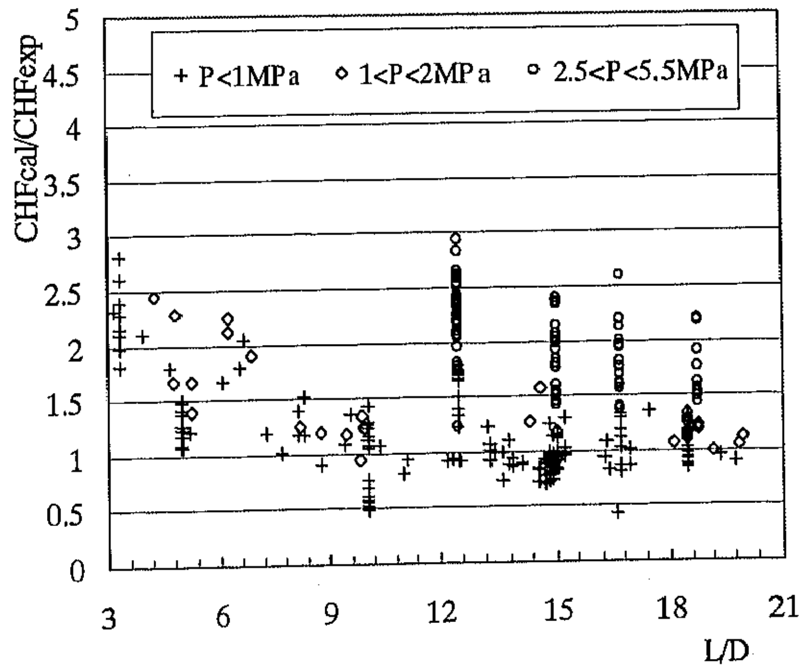

Fig.4-29 CHF Predictions Analysis for Low L/D Data

(1) At low pressure, the over-prediction tendency is not obvious until the L/D reaches extremely low value (L/D<5 at P=0.1MPa).

(2) With the increase of the pressure, the over-prediction tendency turns to be more significant.

(2a) Under the same L/D value, the higher the pressure, the higher the over prediction.

(2b) With the increase of pressure, the over-prediction tendency begins to appear at higher L/D value.

The possible reasons for the over prediction tendency at low L/D condition are analyzed as:

(1) The error in the calculations of the NVG point, exit true quality and void fraction.

As we know, the correlations we used in the present model for the calculations of the NVG point, true quality and void fraction are something empirical and were developed for the thermal hydraulic fully developed region. So, their suitability at low L/D condition, where thermal hydraulic is far from fully developed, is quite doubtful. Actually, with careful model selections for the true quality and void fraction, the present model prediction ability for low L/D data can be improved a lot. For example, as shown in fig. 4-30, by replacing the Ahmad models for the true quality and void fraction with Jafri model (1998, for true quality) and Dix model (1971, for void fraction) respectively, the present model shows a better prediction ability for the low L/D data.

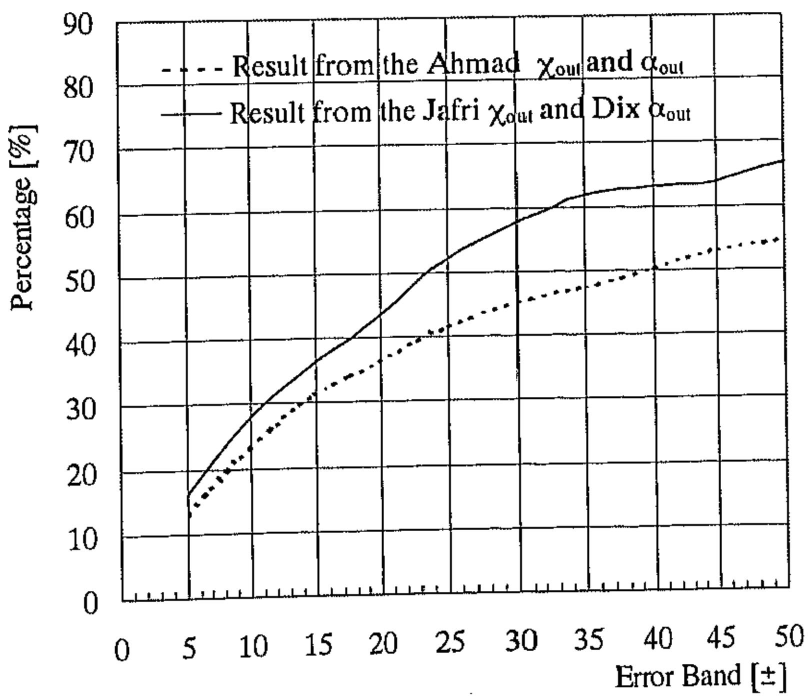

Fig.4-30 CHF Predictions for Low L/D Data with Different Model Adoptions for the True Quality and Void Fraction

(2) The change of the triggering mechanism for the CHF occurrence.

The low L/D condition always results in high CHF (discussed in chapter 4.4, fig.4-36). The high heat flux near the critical condition is considered may easily trigger the happening of the second kind of flow pattern, which, consequently, causes the change of the CHF triggering mechanism (Discussed in chapter 6.3).

As shown in fig.4-31, the present model shows significant ability for the non- low-L/D data prediction. With still the above three databases (totally 2482 points), with omitting the low L/D data (L/D <20, totally 283 points), about 35.8% of data points are predicted within ±5%, 59.7% are predicted within ±10% and about 96% are predicted within ±35%. The R.M.S is about 17.4%.

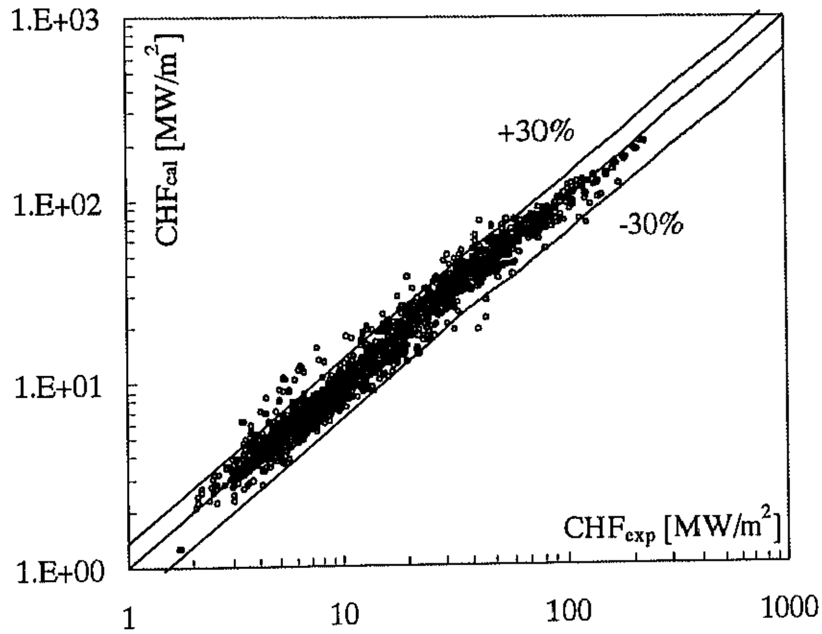

Fig.4-31 Calculated versus Experimental CHF for Non-Low L/D Data

4.4 Parametric Trends of the CHF

As we know, the CHF is function of thermal hydraulic conditions (mass flux, pressure and subcooling) and geometric parameters (inner diameter and ratio of length to diameter). Recently, Celata (1998) investigated the parametric trends of the CHF in terms of the mass flux, pressure, subcooling, channel diameter and heated length from experimental viewpoint. This paper intends to study parametric trends from the model theory viewpoint, with the aim of not only indicating the parametric trends, but also giving the reason for the trends. Experimental data are plotted for comparison if corresponding data are available.

4.4.1 The Thermal Hydraulic Conditions (G, P and ΔT_{in})

The mass flux G, pressure P and inlet subcooling effects on the CHF have been investigated a lot. It is well known that the CHF is an increasing function of the mass flux and inlet subcooling. From the present model, we can see that the increase of the mass flux and inlet subcooling can directly ameliorate exit bulk thermal condition (decrease χ_{out}, α_{out} and T_{lout}) and so make the tube be able to endure a higher heat flux. Figures 4-32 and 4-33 give out the calculated CHF tendencies versus the mass flux and the inlet subcooling respectively. The model shows providing the same observed experimental trend versus the mass velocity and the inlet subcooling.

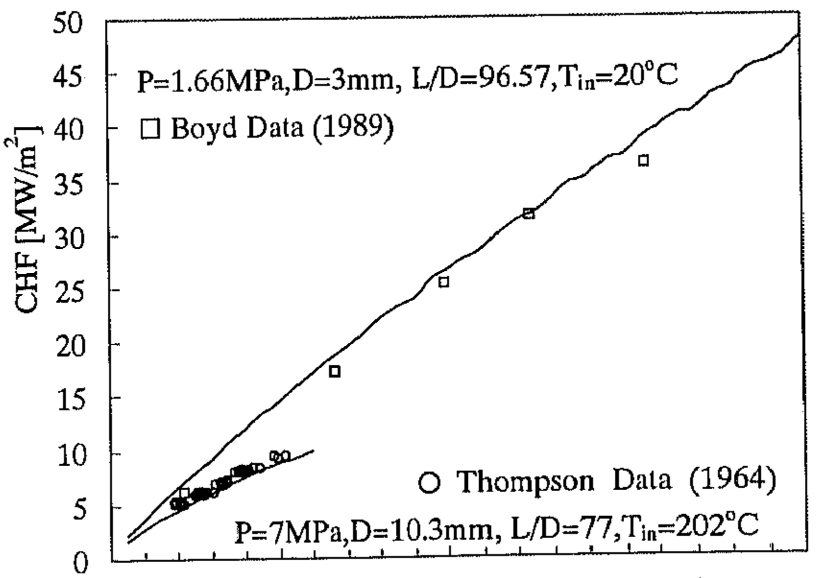

Fig.4-32 Mass Flux Effect on the CHF

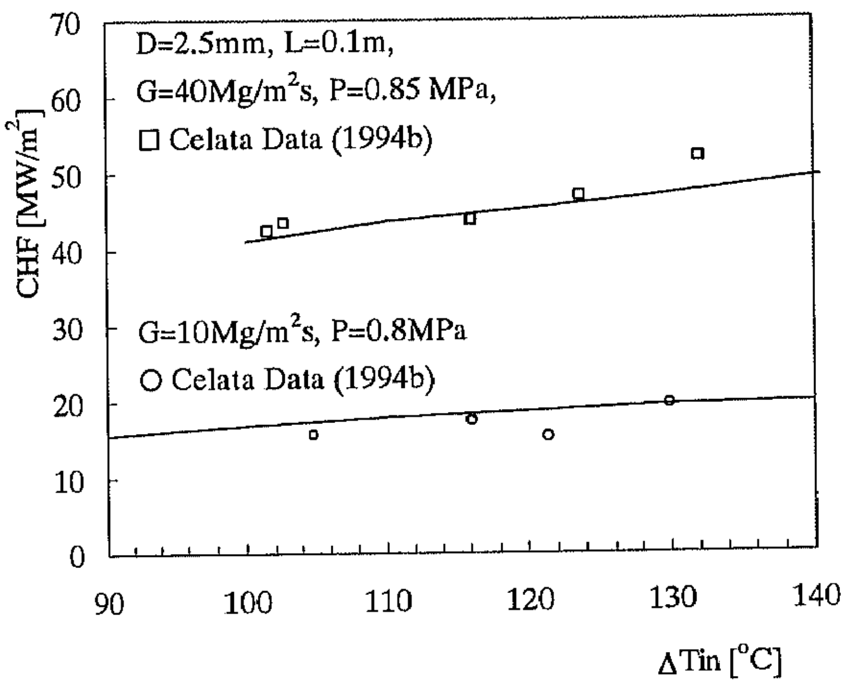

Fig.4-33 Inlet Subcooling Effect on the CHF

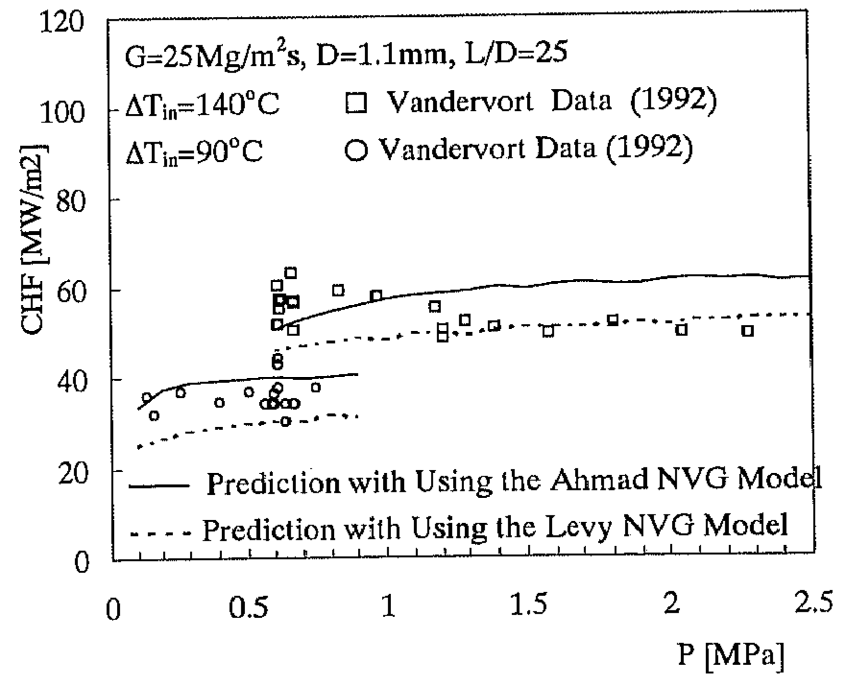

Fig.4-34 Pressure Effect on the CHF

It also has been well accepted that in subcooled flow boiling, the CHF has little relation with the pressure. Fig.4-34 shows the pressure effect on the CHF with using both the Ahmad NVG model and the Levy NVG model represented by solid line and broken line respectively.

Although the proposed model shows predicting right pressure effects on the CHF with employing either the NVG models, generally, the using of the Ahmad model shows a higher CHF prediction tendency than the using of the Levy NVG model.

4.4.2 The Geometric Parameters (D and L/D)

Paying a little attention to the model calculation procedures, we can find that the every appearance of the heated length L is accompanied by the appearance of the inner diameter D (eqs.3-7a, 3-7h). They work together to affect CHF prediction with the form of L/D. So, it's reasonable to use the ratio of the heated length to the inside diameter L/D, as a characteristic parameter. This makes that in the discussion of D effect on the CHF, it's L/D, not L, should be kept as a certain value. Otherwise the shown effect would be the effects from both D and L/D. Same attention should be paid in the discussion of the L/D effect on the CHF.

4.4.2.1 Inner Diameter D

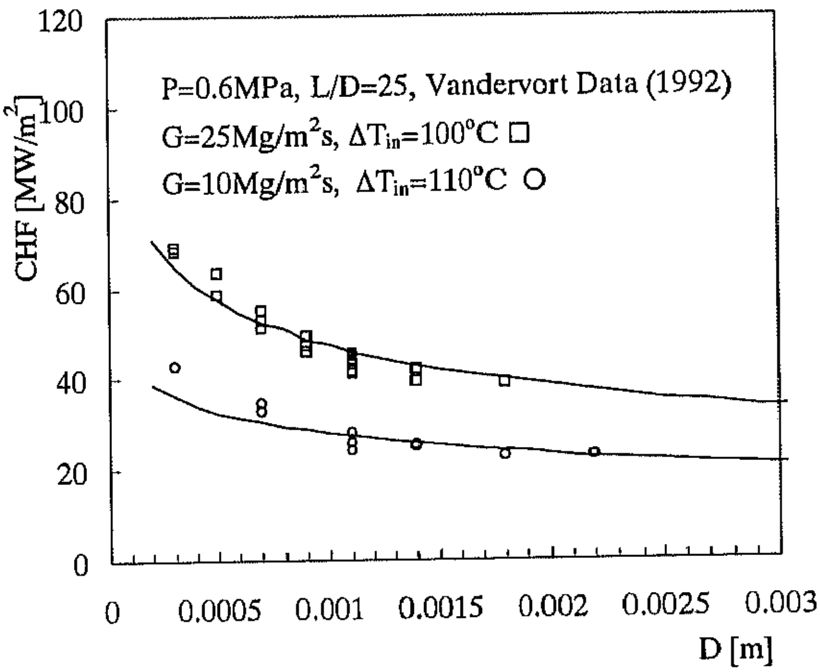

Fig.4-35 Inner Diameter Effect on the CHF

The D effect on the CHF had been discussed a lot. The thought that CHF is an inverse function of the inner diameter has been accepted widely. Figure 4-35 shows the calculated CHF versus the diameter, with plotting in Vandervort experimental data (1992). The model shows to provide the same experimental trend of CHF versus inner diameter D. From the model theory, the trend can be explained as:

A smaller D increases subcooled liquid heat transfer coefficient, defers the NVG point (decrease ΔT_d and increase χ_d) and so ameliorates the exit thermal condition through:

1. Decrease the exit true quality and void fraction.
2. Decrease the exit fluid bulk temperature.

4.4.2.2 The Ratio of the Heated Length to the Inner Diameter L/D

Nariai et al (1987) did an experimental research to seek the L/D effect on CHF at different inner diameter. Figure 4-36 shows the CHF versus L/D from the present model for three different inner diameter conditions. The present model predictions coincide the exp. data quite well. The inflection point in the present model prediction curve is thought as the result of substituting the ΔT_d by the ΔT_{in} when the calculated ΔT_d is higher than ΔT_{in}, which means the NVG occurring at the tube inlet. The phenomenon happens at almost all low L/D conditions. As a whole, the L/D effect on CHF can be concluded as:

For a certain condition, there exists a threshold, beyond which the L/D does little effect on the CHF while inside which the CHF increases significantly as L/D decreases.

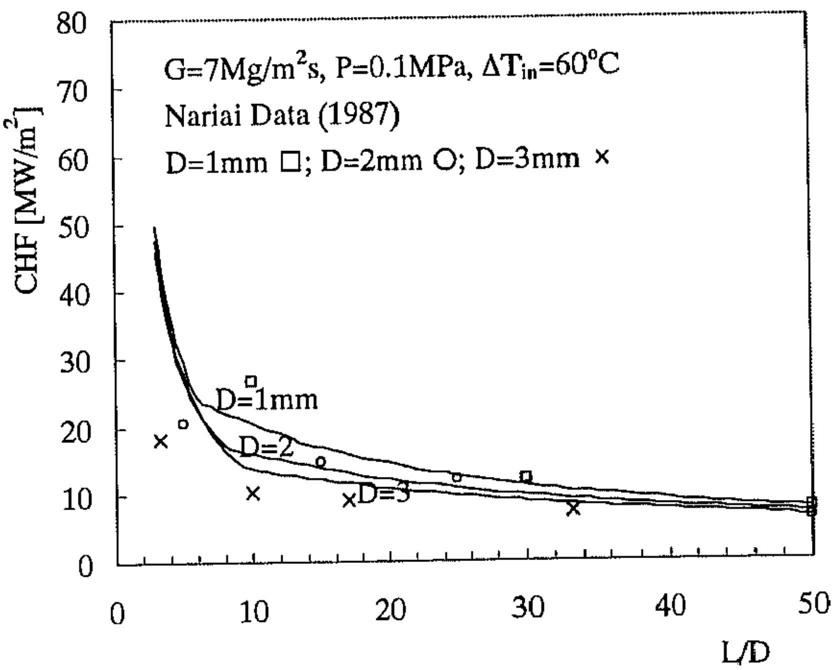

Fig.4-36 L/D Effect on the CHF

From the proposed model calculation process, L/D seems giving a comprehensive and significant effect on CHF. The change of L/D will directly affect χ_{eqout} (eq.3-7a) (which in turn affect χ_{out} (eq.3-7), α_{out} (eq.3-5)) and ΔT_{lout} (eqs.3-7e, 3-7h). We can see clearly that the decrease of L/D will decrease χ_{eqout} and increase ΔT_{lout}, ameliorate the tube exit working condition and so makes the tube be able to endure a higher heat flux.

Seeing eq.3-7a, we get that L/D affect the exit quality and void fraction through its effect on exit equilibrium quality. Figure 4-37 shows L/D effect on χ_d, χ_{eqout}, χ_{out} and α_{out} in the scope of 8<L/D<47 (with L/D<8, χ_{eqout} is lower than χ_d, which means the NVG is not reached at the tube exit; with L/D>47, χ_{eqout} turns to an positive value which means the exit reaches the saturation boiling). Except χ_d keeps as a constant (which has been discussed, only is a function of D and has no relation with the heated length), χ_{eqout}, χ_{out} and α_{out} increase with the increase of L/D. Especially, exit void fraction increases significantly. But the increasing tendency slows down gradually. This is considered as the main reason for the L/D threshold effect on the CHF.

Besides affecting the exit quality and void fraction, as we have mentioned, L/D also affects exit liquid temperature. From eq.3-7h, we get that A increases with the increase of L/D. Then the exit liquid subcooling ΔT_{lout} decreases (eq.3-7e). This is considered as another reason for the L/D effect on the CHF.

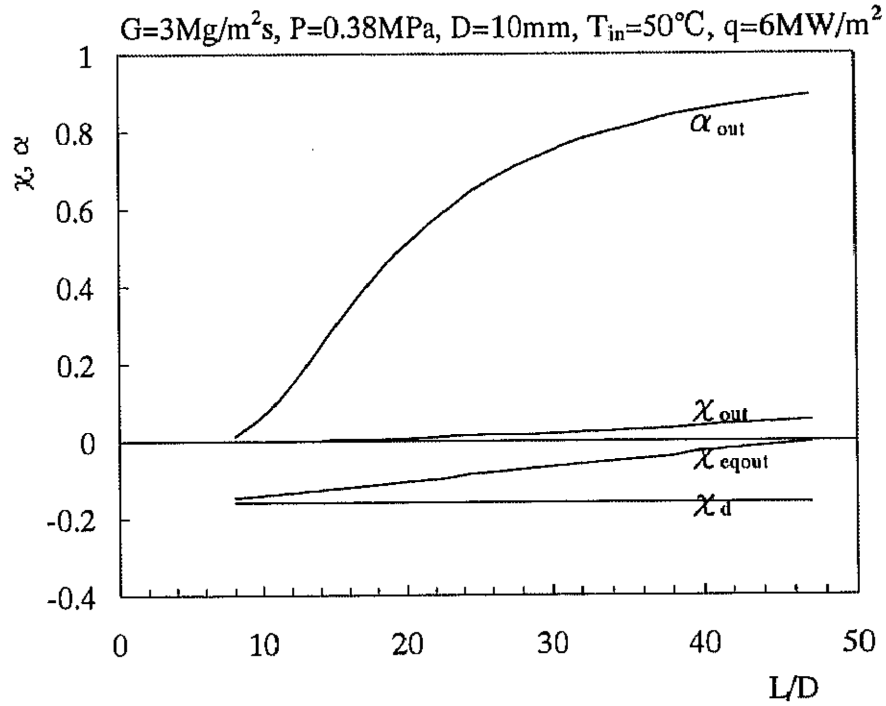

Fig.4-37 L/D Effect on the χ_d, χ_{eqout}, χ_{out} and α_{out}